THIS MONTH IN

JNM

Radioembolization dosimetry: Traino and colleagues offer an overview of locoregional ^{90}Y radioembolization techniques and absorbed doses in liver tumors, providing background and context for a related article in this issue of *JNM*. . . . . ***Page 509***

Breast tumor blood flow: Cochet and colleagues use ^{18}F-FDG PET to evaluate the relationship of tumor blood flow and glucose metabolism with angiogenesis and proliferation markers in newly diagnosed breast cancer . . . . . ***Page 512***

PET and CT perfusion in NSCLC: Sauter and colleagues investigate correlations between glucose metabolism registered by ^{18}F-FDG PET/CT and tumor perfusion quantified by volume perfusion CT and immunohistochemical markers in patients with non–small cell lung cancer. . . . . ***Page 521***

PET as surrogate biomarker in NSCLC: Bengtsson and colleagues assess the predictive value of early-treatment ^{18}F-FDG PET for overall survival in non–small cell lung cancer patients treated with a targeted drug. . . . . ***Page 530***

^{11}C-acetate in localized prostate cancer: Mena and colleagues compare ^{11}C-acetate PET/CT in prostate cancer, benign prostate hyperplasia, and normal prostate tissue with results from multiparametric MRI, whole-mount histopathology, and clinical markers . . . . . ***Page 538***

Parametric PET/MRI: Park and colleagues report on the performance of parametric fusion PET/MRI based on ^{11}C-choline PET/CT and apparent diffusion coefficient MRI maps for identification of primary prostate cancer. . . . . ***Page 546***

Amino acid PET cost effectiveness: Heinzel and colleagues analyze the practical aspects of clinical use of amino acid PET, compared with MRI alone, for surgical resection of high-grade gliomas, from the perspective of the German health insurance system. . . . . ***Page 552***

Artery-specific SPECT/CT partition model: Kao and colleagues describe and validate an image-guided personalized predictive dosimetric technique for ^{90}Y radioembolization, integrating catheter-directed CT hepatic angiography, ^{99m}Tc-macroaggregated albumin SPECT/CT, and partition modeling. . . . . ***Page 559***

PET and GIST therapy: Van den Abbeele and colleagues explore correlations between metabolic response assessed by ^{18}F-FDG PET and objective response, glucose transporter type 4 expression, and genotype in patients with gastrointestinal stromal tumors undergoing neoadjuvant imatinib mesylate therapy. . . . . ***Page 567***

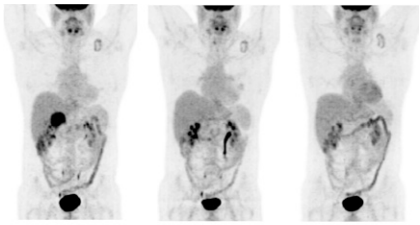

Coronary artery plaque metabolic imaging: Cheng and colleagues use coregistered PET and coronary CT angiography to examine ^{18}F-FDG uptake at culprit sites of acute myocardial infarction after percutaneous coronary stenting. . . . . ***Page 575***

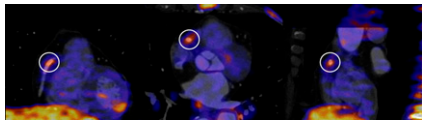

SPECT vs. MRI in cardiomyopathy: Xie and colleagues compare electrocardiogram-gated blood-pool SPECT for assessment of left and right ventricular ejection fractions, end-diastolic volumes, and end-systolic volumes with MRI results in patients with dilated cardiomyopathy. . . . . ***Page 584***

PET indices for AD: Caroli and colleagues compare the relative abilities of three ^{18}F-FDG PET data analysis techniques to distinguish patients with early Alzheimer disease dementia or progressive mild cognitive impairment from cognitively normal adults. . . . . ***Page 592***

PET and endotoxin administration: Hannestad and colleagues use ^{18}F-FDG PET to identify human brain regions involved in the response to endotoxin administration, with results that enhance understanding of the relationship between depression and systemic inflammation . . . . . ***Page 601***

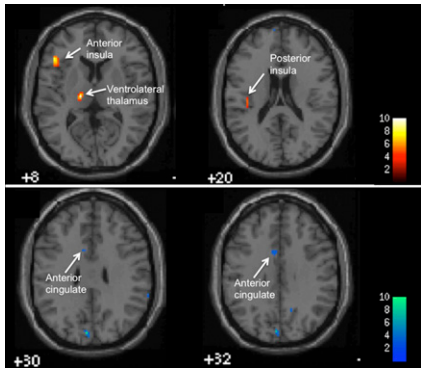

SiPM PET/MRI: Yoon and colleagues describe the development and architecture of a system based on multichannel silicone photomultiplier arrays to allow simultaneous MRI and PET. . . . . ***Page 608***

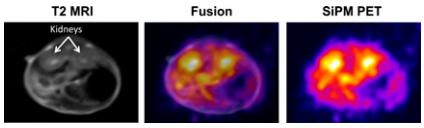

PET marrow RIT dosimetry: Schwartz and colleagues detail and validate a method for directly estimating red marrow activity concentration and self-dose components of absorbed radiation dose to red marrow in radiotherapy, based on PET/CT of two ^{124}I-labeled antibodies . . . . . ***Page 615***

Improving ^{11}C-PiB PET quantification: Zhou and colleagues use a recently developed relative equilibrium–based graphical plot method to enhance and simplify the 2 most commonly used methods for quantification of ^{11}C-Pittsburgh compound B PET . . . . . ***Page 622***

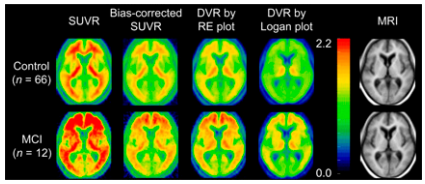

PET and trastuzumab response: Kramer-Marek and colleagues describe a small-animal study on the ability of ^{18}F-FBEM PET Affibody imaging to quantify changes in receptor expression and to predict responses to trastuzumab therapy . . . . . ***Page 629***

Imaging diverse disease biomarkers: Busch and colleagues detail an in vivo spectral multiplexing approach for monitoring interactions among different molecules via near-infrared fluorescent Förster resonance energy, with implications in inflammation, cancer, and neurodegenerative diseases . . . . . ***Page 638***

HSV1716 and ^{131}I-MIBG therapy: Sorensen and colleagues report on the development of noradrenaline transporter gene–infected cells for combined targeted radiotherapy . . . . . ***Page 647***

MI training for NM residents: Graham and Jacene review recent curriculum recommendations for residency training in molecular imaging and nuclear medicine . . . . . ***Page 655***

ON THE COVER

Image-guided personalized predictive dosimetry by artery-specific SPECT/CT partition modeling has been shown to achieve high clinical success rates for safe and effective ^{90}Y radioembolization. In the example illustrated, sublesional dosimetry with left radioembolization lobectomy intent was performed for a patient with recurrent hepatocellular carcinoma.

See page 563.